




AKADÉMIAI KIADÓ

# Impact of wall roughness elements type and height on heat transfer inside a cavity

Issa Omle<sup>1,2,3\*</sup> , Ali Habeeb Askar<sup>1,2,4</sup> and Endre Kovács<sup>2</sup>

Pollack Periodica •  
An International Journal  
for Engineering and  
Information Sciences

19 (2024) 2, 146–153

DOI:  
[10.1556/606.2024.00986](https://doi.org/10.1556/606.2024.00986)  
© 2024 The Author(s)

<sup>1</sup> Department of Fluid and Heat Engineering, Faculty of Mechanical Engineering and Informatics, University of Miskolc, Miskolc-Egyetemvaros, Hungary

<sup>2</sup> Institute of Physics and Electrical Engineering, Faculty of Mechanical Engineering and Informatics, University of Miskolc, Miskolc-Egyetemvaros, Hungary

<sup>3</sup> Department of Mechanical Power Engineering, Faculty of Mechanical and Electrical Engineering, Al-Baath University, Homs, Syria

<sup>4</sup> Department of Mechanical Engineering, Faculty of Mechanical Engineering, University of Technology – Iraq, Baghdad, Iraq

Received: November 17, 2023 • Revised manuscript received: January 20, 2024 • Accepted: January 21, 2024  
Published online: February 13, 2024

## ORIGINAL RESEARCH PAPER



### ABSTRACT

This work investigates the effect of two wall roughness types, triangular and circular, on convection and radiation heat transfer in a small space. The ANSYS Fluent is used to do thermal and dynamic modeling; the left wall is warmer than the right one. The upper and lower walls are adiabatic. The Nusselt numbers are compared in all cases and for two Rayleigh values, which change based on the cavity's characteristic length. The results show temperature contours and Nusselt curves. It was observed that the roughness had a strong effect on the air's thermal behavior inside the cavity, where the Nusselt decreased in both roughness cases, especially at small heights. However, the largest decrease is in the triangular case and for angles less than 90°. For 72°, Nusselt is 13.32 and 6% less than smooth and circular cases respectively.

### KEYWORDS

surface roughness, triangular, circular, Rayleigh number, Nusselt number, heat transfer

## 1. INTRODUCTION

Natural convection in square cavities has been extensively studied because of its numerous uses, but the relationship between surface radiation and natural convection is rarely discussed. Moreover, cavities with smoother walls were the subject of earlier experimental [1] and numerical [2, 3] investigations. The convection of air in a square enclosure with partly thermally active side walls was studied using 2D simulations. Some studies [4, 5] considered a cavity with basic geometry and showed the structure of the flow field and energy within this cavity. The radiological models included in the Fluent 6.3 program were examined and study the impact it in Computational Fluid Dynamics (CFD) simulations of convection heat transfer in a side heated square cavity in to identify the model produces results that are most similar to experimental data [6]. Upon seeing that the velocity patterns on the  $y$ -axis of the radiation-free and radiation-exposed instances varied significantly, it was concluded that the radiation-free case's physical model was rather non-physical. Additionally, the researcher discovered that the S2S model has the best convergence with the experimental data when compared to the models in Fluent 6.3. The studies [7, 8] investigated the interplay of surface radiation with turbulent convection in a chamber with smooth walls. In the Rayleigh number range taken into consideration, it was demonstrated that radiation alters the overall heat transfer by 20% for emissivity  $\varepsilon = 0.2$  and by 60% for  $\varepsilon = 1$ . Rough surfaces have been frequently used as an effective means of enhancing heat transfer efficiency in turbulent

\*Corresponding author.  
E-mail: [omle.issa.jasem@student.uni-miskolc.hu](mailto:omle.issa.jasem@student.uni-miskolc.hu), [issa.j.omle@gmail.com](mailto:issa.j.omle@gmail.com)

thermal convection. However, roughness is not always associated with improved heat transfer and can, on occasion, result in a decrease in the system’s total heat transfer. The simulations are performed in two and three dimensions for Rayleigh numbers ( $Ra = 10^7-10^{11}$ ). The Nusselt number decreased at a fixed Raleigh number regarding little roughness height  $h$ , whereas the heat transfer rate increased for large  $h$  [9].

A study [10] examined the effects of a wall with a sinusoidal wave pattern on convection in 2D within a cavity that held nanofluid. The governing equations for the Finite Volume Method (FVM) discretized velocity field and heat transfer are solved with Semi-Infinite Method for Pursuer Linked Equation (SIMPLE). The data show that Volume Fraction (VF), which doubles the Nusselt number as VF grows from 0 to 0.04, has the most effect on heat transfer. Heat transfer by convection in a porous square cavity with a wavy wall and a partially heated bottom surface was examined using the energy-flux-vector method. Modified Darcy, Rayleigh, Prandtl, and partially heated bottom surface lengths have an effect on the mean Nusselt number and energy-flux-vector distribution. Recirculation zones and a high mean Nusselt number are caused by energy flow vectors when the modified Darcy and Rayleigh numbers are high [11, 12].

As a result, these studies illustrate the lack of data and the extreme dispersion of the configurations and methodology used to simulate convection and radiation heat transfer inside square cavities especially if one of the cavity’s walls is rough. In the previous work [13], the impact of different angles of surface triangle roughness on the interaction between radiation and convection in a cavity is studied. So, to study the impact of surface roughness on the rate of heat transfer in the cavities, this work aims to enrich the database with natural convection and surface radiation coupling inside square cavities containing rough surfaces arranged a triangular and circular shapes.

Now the effect of the shape of the rough surface, whether triangular or circular, is studied on heat transfer by convection and radiation inside square cavities at different Rayleigh numbers and emissivity values using the ANSYS Fluent 19.2 program. First, the triangular surface with different angles and the circular surface with constant radii of surface are compared. Second, the triangular surface with a constant angle of triangle and a different height  $h$  and the circular surface with different radii of surface are compared to study the effect of the height of the rough element on heat transfer. Then, the results are compared with those of surfaces without roughness to see which surface most effectively reduces the amount of heat flowing through it.

## 2. PROBLEM DESCRIPTION

### 2.1. The geometry

The three-dimensional (3D) cavity is shown in Fig. 1; while the cavity’s height  $H$  and length  $W$  are changed, the aspect ratio  $AR = H/W$  stays unchanged. The depth is  $L$ , and  $H_1, H_2$  are the changing dimensions depending on the vertex

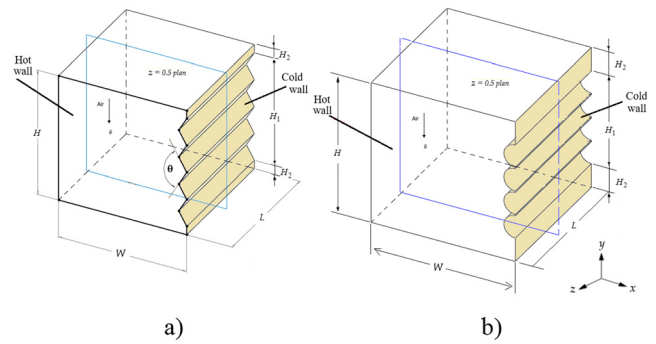


Fig. 1. Diagram in 3D of the geometry for walls with a) triangular roughness and b) circular roughness

angle change  $\theta$ . As the direction of heat transfer is perpendicular to the surface, the problem is regarded as two-dimensional (2D), so the  $z = 0.5$  plane is taken as it is shown in Fig. 2, with changes in the third dimension considered minimal [8]. The 3D effects are disregarded in favor of 2D simulations to reduce the time cost of this study, as evidenced by earlier research [14–18]. Table 1 and Fig. 2 show the boundary conditions of the cavities.

The following are the approximations and hypotheses of the study:

1. Heat transfer by radiation and convection are examined in the cavities;
2. Air fills the cavity, and the Boussinesq buoyancy hypothesis is adopted;
3. The four inner walls of the cavity are considered to be diffuse, gray, opaque, and to have identical emissivity  $\epsilon$  with values listed in Table 1;
4. It is a steady-state study, meaning that  $\partial u/\partial t = 0$  and  $\partial v/\partial t = 0$ ;
5. The physical properties of the air-fluid at the average temperature, which are shown in Table 2, are considered to remain constant, while density varies according to the Boussinesq model;

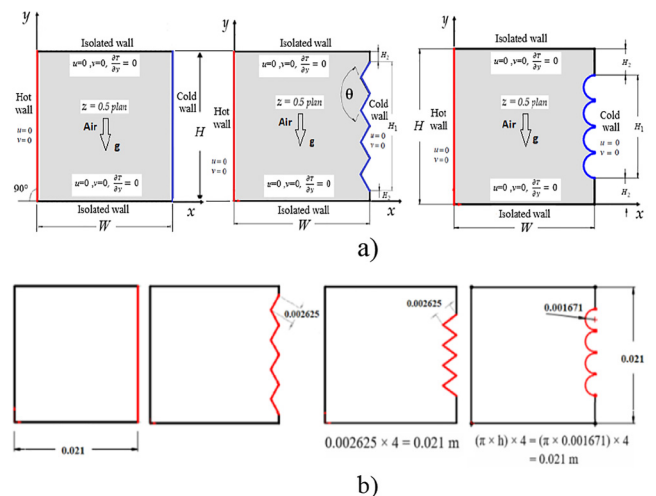


Fig. 2. a) The  $z = 0.5$  plane with boundary conditions, b) shows an example of the triangular and circular walls, and it shows the surface remains constant when the angle is changed

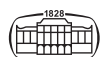


Table 1. The boundary conditions of examined cavities

Wall location	Type condition	Wall Properties					
		The surfaces			Emissivity $\epsilon$		
Right	Cold	$T_c = 288.5$ K	No slip, $u = 0, v = 0$	0	0.4	0.8	1
Left	Hot	$T_h = 298.5$ K	No slip, $u = 0, v = 0$				
Lower	Adiabatic	$\partial T/\partial y = 0$	No slip, $u = 0, v = 0$				
Upper	Adiabatic	$\partial T/\partial y = 0$	No slip, $u = 0, v = 0$				

Table 2. Physical properties of air at average temperature  $T_m = 293.5$  K, based on [8]

Name	Symbol	Value	Unit
Thermal conductivity coefficient	$k$	0.0249	W/(m·K)
Density	$\rho$	1.232	kg/m <sup>3</sup>
Specific heat	$c$	1,008	J/(kg K)
Kinematic viscosity	$\nu$	$1.43 \cdot 10^{-5}$	m <sup>2</sup> /s
Dynamic viscosity	$\mu$	$1.761 \cdot 10^{-5}$	kg/(ms)
Thermal expansion coefficient	$\beta$	0.0034	K <sup>-1</sup>
Thermal diffusivity	$\alpha$	$2 \cdot 10^{-5}$	m <sup>2</sup> /s
Prandtl number	$Pr$	0.71	-
Temperature difference	$\Delta T$	10	K
Average temperature	$T_m$	293.5	K

- In order to facilitate comparison with the reference study results [7], non-dimensional results are provided. Two cavity  $W$  lengths were selected, indicating two distinct Rayleigh numbers. As it is shown in Table 3, the definition of the aspect ratio, or dimensionless square body's adiabatic size, is  $AR = H/W$ ;
- It is a steady-state study, meaning that  $\partial u/\partial t = 0$  and  $\partial v/\partial t = 0$ .

2.2. Solution methods

According to the definition of computational fluid dynamics, this field of study deals with the numerical mathematical techniques used to solve flow and heat transfer equations. As computer technology advanced, it became possible to solve a system of millions of equations with millions of unknowns at a reasonable calculation cost, and this science's general principle is summarized according to Fig. 3 [19].

In this branch of science, the studied space, which includes the area occupied by the fluid, is divided into a finite number of small cells in accordance with the so-called mesh. The equations governing the flow are written for each cell (the physical model), and the differential equations become converted into a set of linear algebraic equations in accordance with the so-called discretization before being solved for all cells [19].

Table 3. Rayleigh numbers depending on characteristic length  $W$

Ra	$W$ (m)	$H$ (m)	$AR = H/W$
$10^4$	0.021	0.021	1
$10^6$	0.097	0.097	1

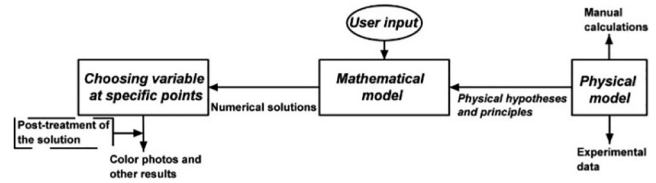


Fig. 3. Scheme of the modeling

The results of the solution are displayed subsequently, either in the form of colored images describing the flow structure or in the form of graphic curves that are analyzed to describe and provide an approximation of what is occurring in the domain. Finally, the model and the solution are validated by comparing these results to experimental data or to the results of earlier studies using a few logical approximations that are related to the numerical solution, for example observing the general convergence criterion and determining the value of a point or surface [20].

2.3. The governing equations

Continuity equation:

$$\frac{\partial u}{\partial x} + \frac{\partial v}{\partial y} + \frac{\partial w}{\partial z} = 0, \tag{1}$$

where  $u$  is the  $x$ -component,  $v$  is the  $y$ -component, and  $w$  is the  $z$ -component of the velocity (m s<sup>-1</sup>), respectively.

The momentum equation on the  $x$ -axis:

$$\rho \left( u \frac{\partial u}{\partial x} + v \frac{\partial v}{\partial y} \right) = -\frac{\partial p}{\partial x} + \mu \left( \frac{\partial^2 u}{\partial x^2} + \frac{\partial^2 v}{\partial y^2} \right), \tag{2}$$

on the  $y$ -axis:

$$\rho \left( u \frac{\partial u}{\partial x} + v \frac{\partial v}{\partial y} \right) = -\frac{\partial p}{\partial x} + \rho g \beta (T - T_\infty) + \mu \left( \frac{\partial^2 u}{\partial x^2} + \frac{\partial^2 v}{\partial y^2} \right), \tag{3}$$

where  $\rho g \beta (T - T_\infty)$  is the buoyancy Boussinesq approximation,  $g$  is the gravitational acceleration of the Earth and equal 9.81 (m s<sup>-2</sup>) [21].

The energy equation

$$\left( u \frac{\partial T}{\partial x} + v \frac{\partial T}{\partial y} \right) = \frac{k}{\rho c} \left( \frac{\partial^2 T}{\partial x^2} + \frac{\partial^2 T}{\partial y^2} \right). \tag{4}$$

The governing equations for natural convection are non-dimensional, and to reduce the total number of variables, they are combined to produce non-dimensional numbers.



The following equations are used to calculate the results in ANSYS Fluent software:

$$Nu_{tot} = Nu_{conv} + Nu_{rad} = \frac{1}{A} \int Nu_{local} \cdot dA, \quad (5)$$

$$Nu_{conv} = \frac{q_{conv} \cdot H \cdot L}{k(T_h - T_c)}, \quad (6)$$

$$Nu_{rad} = \frac{q_{rad} \cdot H \cdot L}{k(T_h - T_c)}, \quad (7)$$

$$q_{tot} = q_{conv} + q_{rad} = \frac{1}{A} \int q_{local} \cdot dA, \quad (8)$$

where  $L = 1$  m, as previously stated.

## 2.4. The dimensionless numbers

The physics formula for the Rayleigh number is the ratio of buoyancy and viscosity forces multiplied by the ratio of momentum and heat diffusivities as following:

$$Ra = \frac{g\beta\Delta TW^3}{\nu\alpha}, \quad (9)$$

where  $W$  is the distance between the cold and hot surfaces, i.e., the characteristic length (m). Below the critical threshold of Rayleigh number, most heat transfer is accounted for via conduction. Convection accounts for the majority of heat transfer above this threshold value.

To determine the heat transfer rate across the cavity's walls, a surface Nusselt number along the cold the cavity's wall was used.

It is the conductive to convective heat transfer ratio across the boundary. Due to the problem's non-dimensional description, the local Nusselt number along the cavity's right wall can be defined as

$$Nu = \frac{hA(T_1 - T_2)}{kA(T_1 - T_2)/W} = \frac{Q_{conv}}{Q_{cond}} = \frac{hW}{k}, \quad (10)$$

where the surface area for heat transfer is  $A$  ( $m^2$ ), and  $h$  is the flow's convective coefficient ( $W/(m^2K)$ ). Consequently, the strength of convective heat transfer in relation to conduction heat transfer through the liquid is indicated by the Nusselt number. So, when the Nusselt number rises, convective heat transfer becomes dominant [22].

The ratio of momentum diffusivity  $\nu$  to thermal diffusivity  $\alpha$  is the definition of the Prandtl number in terms of physics. It provides the measurement of the efficiency of diffusion transport over the thermal and velocity boundary layers as follows:

$$Pr = \frac{\nu}{\alpha}. \quad (11)$$

## 3. THE MESH CONSTRUCTION

According to [23], the fluid's region is divided into a limited number of smaller portions, each known as a cell. After

that, the fundamental flow equations for every cell can be expressed and converted into algebraic form, which can be solved numerically.

As it can be seen in Fig. 4, the investigated domain in the current study was meshed using the ANSYS Meshing Application code. Hexahedral cells were used to create the mesh at the smooth wall, and tetrahedral cells at the rough wall. The refinement feature is used to smooth the mesh near surfaces and correct the gradients associated with the boundary layer for rough walls [24].

More cells lead to a more accurate solution, but this costs a lot of computing power. As the number of cells surpasses a certain threshold, the results stay nearly constant, meaning that so-called mesh independence has been attained [25]. Thus, nine meshes with progressively more elements for the smooth wall are employed to determine whether the results are independent of the mesh density [26]. As it is shown in Table 4, the Nusselt number is computed based on the element numbers on the smooth and rough walls. The Nusselt number does not change when the number of elements is greater than 72,370 and 76,100 for smooth and rough walls cases respectively, as it can be seen in Fig. 5. Thus, 72,370 and 76,100 are the total number of elements selected for both.

A collection of differential equations is converted into a set of linear (algebraic) equations as part of the solution process then solved using a method similar to the numerical solution [27]. The SIMPLE method is used to achieve the correlation and coupling between pressure and velocity in

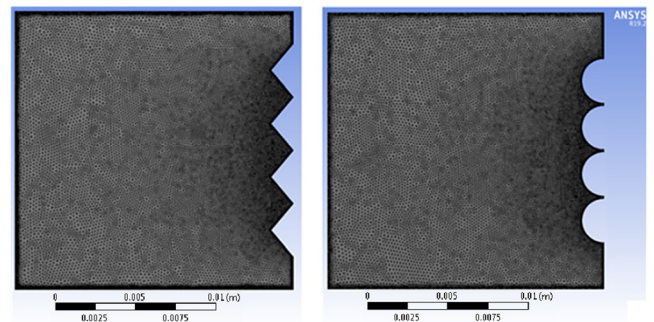
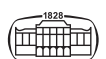


Fig. 4. Shows the mesh used

Table 4. Nusselt numbers based on the number of elements

Smooth		Rough	
Elements	Nu	Elements	Nu
20	2.368	42	2.031
560	2.359	1,008	2.034
6,200	2.344	8,560	2.0486
12,680	2.310	15,800	2.075
26,700	2.300	31,876	2.078
48,160	2.299	55,420	2.080
72,370	2.298	76,100	2.082
98,000	2.298	102,060	2.082
123,400	2.298	130,240	2.082



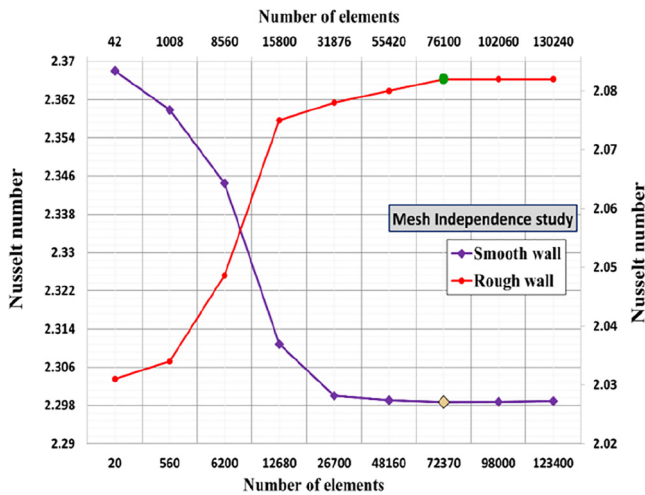


Fig. 5. Total Nusselt number for smooth (left axis) and rough (right axis) walls as a function of number of elements

the continuity and momentum equations. The momentum and energy equations are solved using second-order interpolation. The body force weighted that is suggested in the ANSYS User Guide is applied to the pressure.

## 4. RESULTS AND ANALYSIS

### 4.1. Comparing the $Nu_{total}$ in case of no radiation $\epsilon = 0$

For both Rayleigh numbers  $10^4$  and  $10^6$  and in the case of  $\epsilon = 0$ , the total Nusselt number of circular roughness is smaller than triangular roughness with angles larger than 100, but for angles smaller than  $100^\circ$ , the Nusselt number is large as it is shown in Fig. 6.

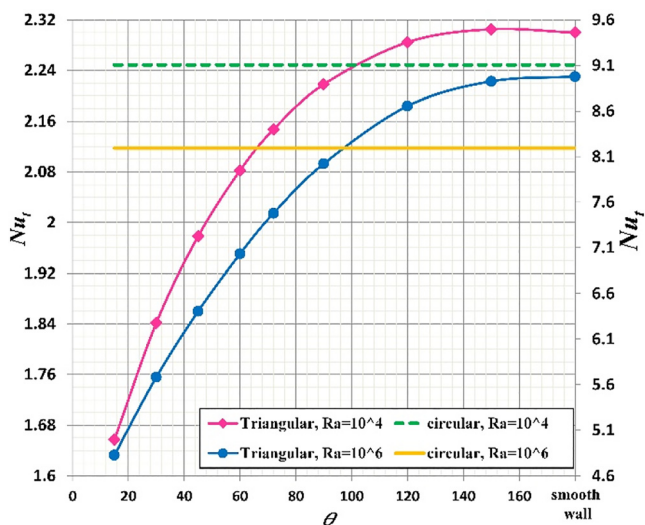


Fig. 6. Comparing the  $Nu_t$  according to the roughness type at  $\epsilon = 0$ , where the left axis refers to  $Nu_t$  at Rayleigh number  $Ra = 10^4$ , and the right one refers to  $Nu_t$  at  $Ra = 10^6$

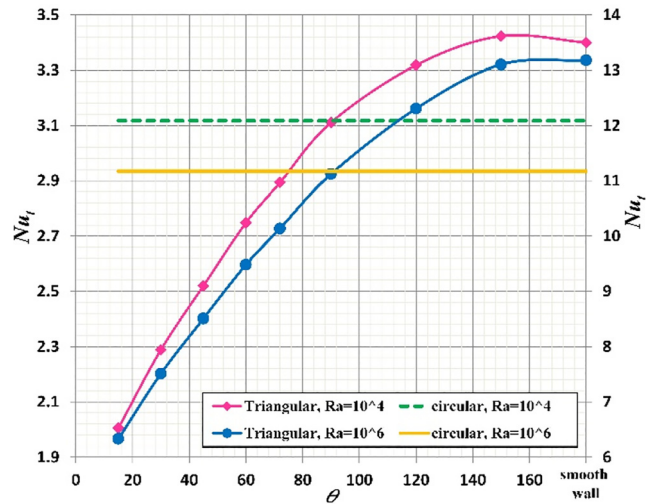


Fig. 7. Comparing the  $Nu_t$  according to the roughness type at  $\epsilon = 0.4$ , where the left axis refers to  $Nu_t$  at Rayleigh number  $Ra = 10^4$ , and the right one refers to  $Nu_t$  at  $Ra = 10^6$

### 4.2. Comparing the $Nu_{total}$ in case of radiation with $\epsilon = 0.4$

The total Nusselt number in the case of the triangular roughness surface at angles greater than  $92^\circ$  and for  $\epsilon = 0.4$  is larger than the circular roughness surface case for Rayleigh number values  $10^4$  and  $10^6$ . However, the total Nusselt number becomes smaller at angles less than  $92^\circ$  for triangular roughness as it is shown in Fig. 7.

### 4.3. Comparing the $Nu_{total}$ in case of radiation with $\epsilon = 0.8$

For stronger radiation  $\epsilon = 0.8$  and for Rayleigh number values  $10^4$  and  $10^6$ , the total Nusselt number in triangular

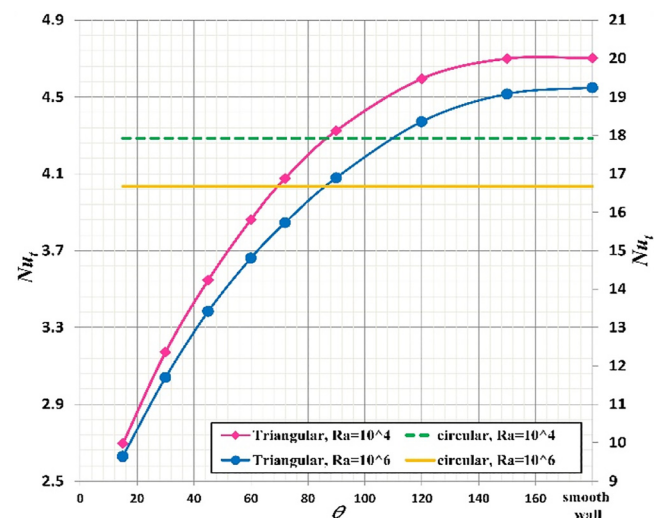


Fig. 8. Comparing the  $Nu_t$  according to the roughness type at  $\epsilon = 0.8$ , where the left axis refers to  $Nu_t$  at Rayleigh number  $Ra = 10^4$ , and the right one refers to  $Nu_t$  at  $Ra = 10^6$



roughness case at angles greater than  $90^\circ$  is larger than the circular roughness surface case, but at angles less than  $90^\circ$ , the total Nusselt number becomes smaller in the case of triangular roughness as it is shown in Fig. 8.

The simulations were repeated at  $\varepsilon = 1$ , it was found the total Nusselt number in the case of the circular roughness is smaller than the triangular one at angles greater than  $88^\circ$ .

From the temperature distribution contours, because the viscous effects become more significant as  $Ra$  decreases, in the case of both types of roughness, the fluid will become

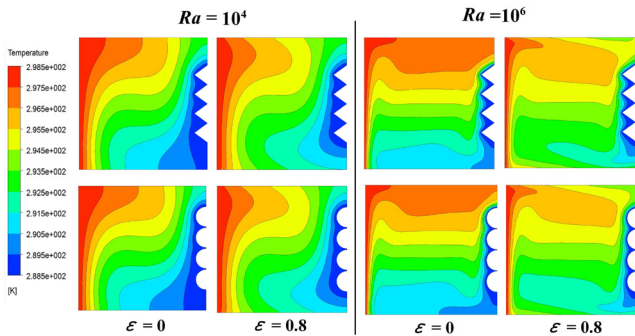


Fig. 9. Temperature distribution contours in the case of circular and triangular rough walls with an angle of  $72^\circ$  for different emissivity

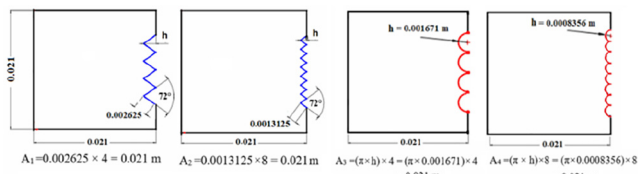


Fig. 10. Shows changing the height of triangular and circular roughening elements with constant area

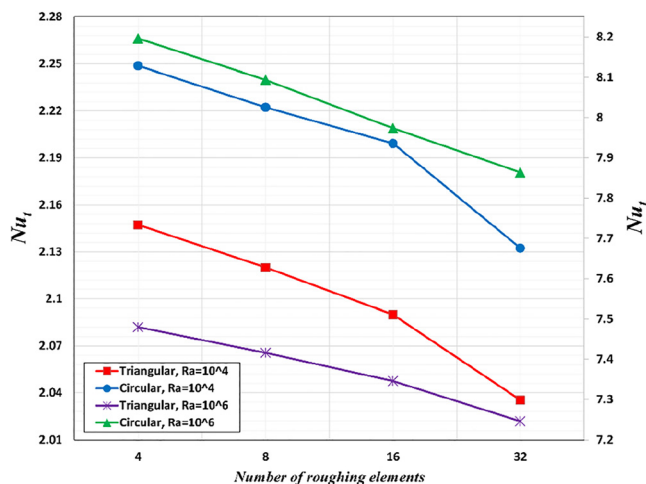


Fig. 11. Shows the  $Nu_t$  as a function of the roughness element numbers at  $\varepsilon = 0$ , where the left axis refers to  $Nu_t$  at Rayleigh number  $Ra = 10^4$ , and the right one refers to  $Nu_t$  at  $Ra = 10^6$

trapped and accumulate inside the hollow regions between the rough elements as it is shown in Fig. 9. As a result, a larger thermal boundary layer is formed, which impedes the system's overall heat flux by reducing convective heat transfer.

#### 4.5. Comparing the $Nu_{total}$ in case of changing the height of roughening elements

Figure 10 shows how the height of circular and triangular roughness elements changes with a constant area.

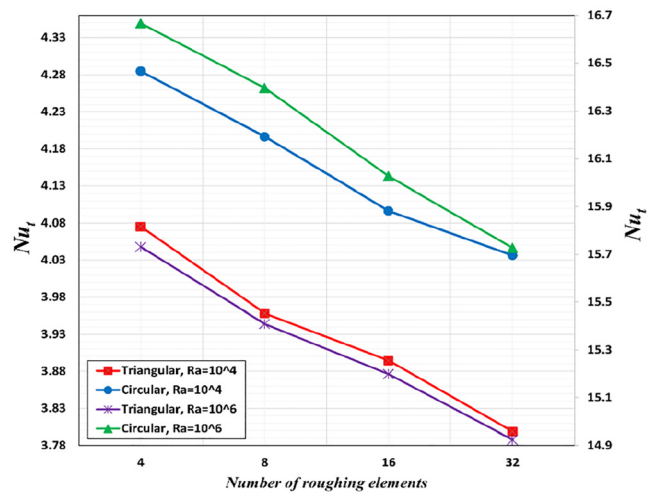


Fig. 12. Shows the  $Nu_t$  as a function of the roughness element numbers at  $\varepsilon = 0.8$ , where the left axis refers to  $Nu_t$  at Rayleigh number  $Ra = 10^4$ , and the right one refers to  $Nu_t$  at  $Ra = 10^6$

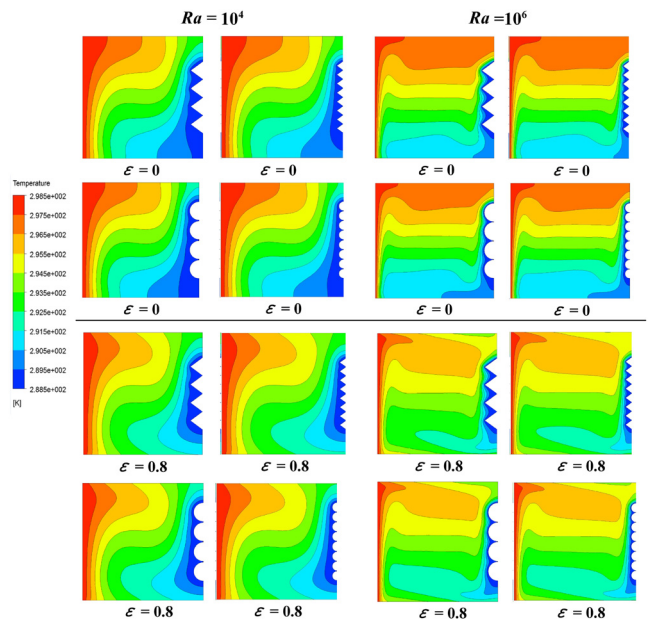
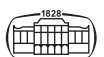


Fig. 13. Temperature distribution contours in the case of changing the roughening height element  $h$  for different emissivity and for both Rayleigh numbers  $10^4$  and  $10^6$



In the case of no radiation with  $\varepsilon = 0$  and radiation with  $\varepsilon = 0.8$ , and for both Rayleigh numbers  $10^4$  and  $10^6$ , the total Nusselt decreases when the number of circular or triangular roughing elements increases and, equivalently, when the height of the roughness element decreases. The total Nusselt number is smaller in the case of triangular roughness compared to circular, as it is shown in Figs 11 and 12. Increasing emissivity and Rayleigh number both lead to an increase in the total Nusselt value.

The temperature contours for different Rayleigh numbers are shown in Fig. 13.

## 5. CONCLUSION

This study focused on examining the impact of surface radiation, how the wall's roughness type affects heat transfer and the thermal and hydrodynamic behavior of a fluid inside the cavity.

Two cavities are investigated for this purpose, implying two distinct Rayleigh numbers. In the case of smooth and rough walls, mesh independence was carried out. As a result, it was found that when the angle of the triangular roughing decreases, the heat transfer rate decreases since there is less buoyancy force at  $Ra = 10^4$ , which could cause the fluid to become trapped in the spaces between the roughness pieces due to the low velocity. A decrease in fluid volume, the formation of vortices near roughness components, and a reduction in the effective distance between two walls could be the main factors influencing fluid flow and overall heat transmission in the cavity.

For the triangular and circular roughness, the total Nusselt decreases when the number of circular or triangular roughing elements increases or, equivalently, when the height of the roughness element decreases. The total Nusselt number is smaller in the case of triangular roughness compared to circular, whereas the rough surface in a circular form is reduced by 8.86% for the Nusselt value from the smooth surface.

Increasing emissivity and Rayleigh number both lead to an increase in the total Nusselt value. The heat transfer rate is low if the surface is roughened in a triangular shape with cross-section angles less than  $85^\circ$  at small heights of the roughness elements.

## REFERENCES

- [1] H. Wang, S. Xin, and P. Le Quéré, "Numerical study of the coupling of natural convection with the radiation of surfaces in square cavities filled with air" (in French), *Comptes Rendus - Mec.*, vol. 334, no. 1, pp. 48–57, 2006.
- [2] E. Abu-Nada and A. J. Chamkha, "Mixed convection flow in a lid-driven inclined square enclosure filled with a nanofluid," *Eur. J. Mech. B/Fluids*, vol. 29, no. 6, pp. 472–482, 2010.
- [3] R. Anandalakshmi and T. Basak, "Natural convection in rhombic enclosures with isothermally heated side or bottom wall: Entropy generation analysis," *Eur. J. Mech. B/Fluids*, vol. 54, pp. 27–44, 2015.
- [4] M. K. Kane, C. Mbow, M. L. Sow, and J. Sarr, "A study on natural convection of air in a square cavity with partially thermally active side walls," *Open J. Fluid Dyn.*, vol. 7, no. 4, pp. 623–641, 2017.
- [5] S. M. Aminossadati and B. Ghasemi, "Natural convection cooling of a localised heat source at the bottom of a nanofluid-filled enclosure," *Eur. J. Mech. B/Fluids*, vol. 28, no. 5, pp. 630–640, 2009.
- [6] S. Thakur and S. Kumar, "Impact of radiation models in CFD simulations of natural convection heat transfer in a side heated square cavity," *Int. J. Res. Appl. Sci. Eng. Technol.*, vol. 4, no. 4, pp. 832–839, 2016.
- [7] Z. Guo, J. Wang, A. K. Mozumder, and P. K. Das, "Mixed convection of nanofluids in a lid-driven rough cavity," in *7th BSME International Conference on Thermal Engineering*, Dhaka, Bangladesh, December 22–24, 2016, vol. 1851, 2017, Art no. 020004.
- [8] N. H. Laaroussi, "Contribution to the numerical simulation of heat transfers by conduction, radiation and thermosolutal convection in cavities" (in French), Doctoral Thesis, University Paris-Est, 2008.
- [9] Y. Z. Zhang, C. Sun, Y. Bao, and Q. Zhou, "How surface roughness reduces heat transport for small roughness heights in turbulent Rayleigh-Bénard convection," *J. Fluid Mech.*, vol. 836, 2018, Art no. R2.
- [10] M. S. Zarei, A. T. K. Abad, M. Hekmatifar, and D. Toghraie, "Heat transfer in a square cavity filled by nanofluid with sinusoidal wavy walls at different wavelengths and amplitudes," *Case Stud. Therm. Eng.*, vol. 34, 2022, Art no. 101970.
- [11] W. Al-Kouz, K. B. Saleem, and A. Chamkha, "Numerical investigation of rarefied gaseous flows in an oblique wavy sided walls square cavity," *Int. Commun. Heat Mass Transf.*, vol. 116, 2020, Art no. 104719.
- [12] M. Hirpho, "Mixed convection of Casson fluid in a differentially heated bottom wavy wall," *Heliyon*, vol. 7, no. 6, 2021, Art no. e07361.
- [13] I. Omle, E. Kovács, and B. Bolló, "The effect of surface triangular roughness inspired by nature with different angles on the interaction between free convection and surface radiation in a square cavity," *Heat Transf. Res.*, vol. 55, no. 5, pp. 1–24, 2024.
- [14] I. Omle, A. H. Askar, E. Kovács, and B. Bolló, "Comparison of the performance of new and traditional numerical methods for long-term simulations of heat transfer in walls with thermal bridges," *Energies*, vol. 16, no. 12, 2023, Art no. 4604.
- [15] B. Yang and C. Lawn, "Fluid dynamic performance of a vertical axis turbine for tidal currents," *Renew. Energy*, vol. 36, no. 12, pp. 3355–3366, 2011.
- [16] R. Lanzafame, S. Mauro, and M. Messina, "2D CFD modeling of H-Darrieus wind turbines using a transition turbulence model," *Energy Proced.*, vol. 45, pp. 131–140, 2014.
- [17] S. McTavish, D. Feszty, and T. Sankar, "Steady and rotating computational fluid dynamics simulations of a novel vertical axis wind turbine for small-scale power generation," *Renew. Energy*, vol. 41, pp. 171–179, 2012.
- [18] A. Sayyed, "Air flow optimization through an intake system for a single cylinder formula student (FSAE) race car," *Int. J. Eng. Res.*, vol. 6, no. 1, pp. 183–188, 2017.



- [19] T. J. Chung, *Computational Fluid Dynamics*. Cambridge University Press, 2002.
- [20] I. Omle, E. Kovács, and B. Bolló, “Applying recent efficient numerical methods for long-term Simulations of heat transfer in walls to optimize thermal insulation,” *Results Eng.*, vol. 20, 2023, Art no. 101476.
- [21] Y. Cengel and A. Ghajar, *Heat and Mass Transfer: Fundamentals and Applications*, McGraw-Hill, 2014.
- [22] J. Holman, *Heat Transfer*, 10th ed. McGraw-Hill, 2010.
- [23] F. Moukalled, L. Mangani, and M. Darwish, *The Finite Volume Method in Computational Fluid Dynamics*. Springer, 2016.
- [24] ANSYS Fluent Theory Guide, 2017.
- [25] O. Al-Oran and F. Lezsovits, “Thermal performance of inserting hybrid nanofluid in parabolic trough collector,” *Pollack Period.*, vol. 16, no. 3, pp. 88–93, 2021.
- [26] M. S. Kamel and F. Lezsovits, “Simulation of nanofluids laminar flow in a vertical channel,” *Pollack Period.*, vol. 13, no. 2, pp. 147–158, 2018.
- [27] J. Strzałkowski, P. Sikora, S. Y. Chung, and M. A. Elrahman, “Thermal performance of building envelopes with structural layers of the same density: Lightweight aggregate concrete versus foamed concrete,” *Building and Environment*, vol. 196, 2021, Art no. 107799.

